Simultaneous Motion Tracking and Joint Stiffness Control of Bidirectional Antagonistic Variable-Stiffness Actuators

Marie Harder[1], Manuel Keppler[1], Xuming Meng[1], Christian Ott[1,2], Hannes Höppner[3], and Alexander Dietrich[1]

***Abstract*—Since safe human-robot interaction is naturally linked to compliance in these robots, this requirement presents a challenge for the positioning accuracy. The class of variable-stiffness robots features intrinsically soft contact behavior where the physical stiffness can even be altered during operation. Here we present a control scheme for bidirectional, antagonistic variable-stiffness actuators that achieve high-precision link-side trajectory tracking while simultaneously ensuring compliance during physical contact. Furthermore, the approach enables to regulate the pretension in the antagonism. The theoretical claims are confirmed by formal analyses of passivity during physical interaction and the proof of uniform asymptotic stability of the desired link-side trajectories. Experiments on the forearm joint of the DLR robot *David* verify the proposed approach.**

***Index Terms*—Motion Control, Compliance and Impedance Control, Compliant Joints and Mechanisms.**

I. Introduction

MODERN robots are supposed to work closely with humans, which is steadily moving physical human-robot interaction and safety more into focus. To protect humans and robots in the event of collisions, inherent compliance can be integrated within the structure of the systems. In series elastic actuators (SEA) [1] a spring with constant elasticity is placed between motor and link, whereas in variable-stiffness actuators (VSA) the stiffness of the elastic element can be deliberately adjusted [2]. Besides increased mechanical robustness against unknown contact forces and impacts, a variety of further advantages of intrinsic compliance within the drive train exist, including aspects such as lower reflected inertias, and energy-storing capabilities, among others. However, these benefits come at the price of intrinsic oscillatory dynamics that increase the control complexity and pose challenges in terms of positioning accuracy and tracking performance.

Within the class of VSA one can distinguish between different design principles [4]. One subcategory includes systems where a large motor controls the joint position while a smaller one is responsible to adjust the stiffness. This concept is, for example, implemented in the shoulder and elbow joints of the DLR robot *David* [5], see Fig. 1, called Floating Spring Joints [6]. In the controller design of such mechanisms, the adjuster dynamics are often neglected [7]. In contrast to that, the effect of both motors is coupled in antagonistic setups, as it is used in the tendon-driven hands of DLR *David*. Depending on the relative motion between the two motors, either the stiffness or the equilibrium position is altered. An extension of the antagonistic setup is the bidirectional antagonistic structure, where both motors are connected bidirectionally to the link [8]–[10]. The authors in [8] presented and analyzed a tendon-driven prototype. This version was improved for the forearm rotation and the two wrist joints of the DLR *David* to a tendon-free mechanism. That is based on harmonic drive gears including floating circular splines with mechanical cam discs pretensioning springs (bidirectional antagonism with variable stiffness (BAVS); [11], [3]). Advantageously, the sum of both motor torques is available at the link side. Yet, due to the coupling in antagonistic setups the motor dynamics of both motors have to be taken into account, which increases the complexity of the control of such mechanisms.

In terms of the control of antagonistic VSA only a few approaches can be found in the literature. In [12] and [13]

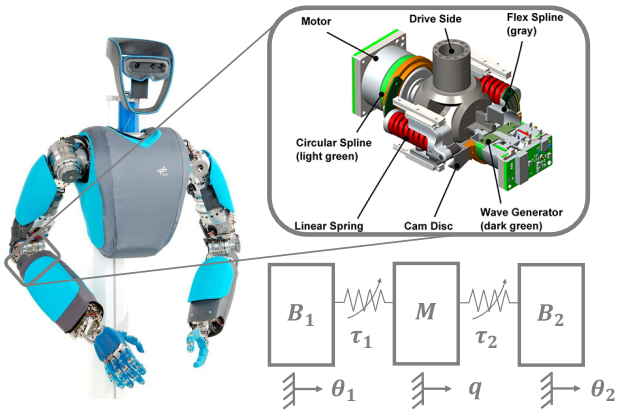

Fig. 1. CAD drawing (top) and schematic representation (bottom) of the bidirectional antagonistic variable stiffness (BAVS) actuation mechanism as it is implemented in the forearm rotation of the DLR *David*. Adapted from [3].

Manuscript received: February, 24, 2022; Accepted April, 27, 2022.

This paper was recommended for publication by Editor J. Kober upon evaluation of the Associate Editor and Reviewers' comments. This work has received funding from the European Research Council (ERC) under the European Union's Horizon 2020 research and innovation programme (grant agreement No. 819358).

[1]The authors are with the Institute of Robotics and Mechatronics, German Aerospace Center (DLR), Wessling, Germany marie.harder@dlr.de

[2]C. Ott is with the Automation and Control Institute at TU Wien, 1040 Wien, Austria ott@acin.tuwien.ac.at

[3]H. Höppner is with the Beuth University of Applied Sciences, Berlin, Germany Hannes.Hoeppner@bht-berlin.de

Digital Object Identifier (DOI): see top of this page.

a control strategy based on static and dynamic feedback-linearization is proposed and validated in simulations. In [14] a simplified model with linearized variable stiffness is used to design a tracking controller based on optimal control principles, and the concept is evaluated in simulation. However, in order to deploy the controller for the simplified model in actual VSA robots, a mapping of the control action from the linearized model to the real system is needed. Based on the feedback equivalence principle a state feedback control law is presented in [15] which ensures dynamic gravity cancellation and set-point regulation. A tracking controller that simultaneously regulates the position and the stiffness is implemented in [16] for a novel class of antagonistic variable stiffness actuators based on equivalent nonlinear torsion springs. The authors transform the state space model into an integral chain-type pseudo-linear system with input saturation constraints. For this system a sliding mode control is designed and validated in simulation [16]. In [17] and [18] the elastic structure preserving (ESP) control approach of [7] was extended to a bidirectional antagonism with variable stiffness. However, only the regulation control problem was addressed.

In this work we present a link-side tracking controller for BAVS mechanisms. Moreover, the approach enables to simultaneously control a desired pretension of the elastic elements. Two formal proofs are provided to substantiate the theoretical properties of the proposed concept: uniform asymptotic stability of the desired link-side trajectory is shown, and a proof of passivity is provided to attest proper interaction behavior during physical contact with the controlled robot. The control strategy is validated and the theoretical claims are confirmed in experiments on the lower-arm BAVS joint of the DLR *David* robot, see Fig. 1.

The article is organized as follows: After the controller design in Section II, passivity and stability are formally analyzed in Section III and Section IV, respectively. The experimental validation is conducted in Section V, followed by the conclusion in Section VI.

II. Controller Design

A. Control Objectives

In this paper a robot with n degrees of freedom (DoF) and only BAVS joints is considered. A simplified model of the elastic robot is considered as proposed in [19], where it is assumed that the kinetic energy of a rotor is mainly due to its own angular velocity, which can be justified for high gear ratios. That leads to the following system dynamics:

$$\boldsymbol{M}(\boldsymbol{q})\ddot{\boldsymbol{q}} + \boldsymbol{C}(\boldsymbol{q},\dot{\boldsymbol{q}})\dot{\boldsymbol{q}} + \boldsymbol{g}(\boldsymbol{q}) = \boldsymbol{\tau}_1(\boldsymbol{\varphi}_1^\theta) + \boldsymbol{\tau}_2(\boldsymbol{\varphi}_2^\theta) + \boldsymbol{\tau}_{\text{ext}} \tag{1}$$

$$\boldsymbol{B}_1\ddot{\boldsymbol{\theta}}_1 + \boldsymbol{\tau}_1(\boldsymbol{\varphi}_1^\theta) = \boldsymbol{u}_1 \tag{2}$$

$$\boldsymbol{B}_2\ddot{\boldsymbol{\theta}}_2 + \boldsymbol{\tau}_2(\boldsymbol{\varphi}_2^\theta) = \boldsymbol{u}_2 \tag{3}$$

Herein, $\boldsymbol{q},\dot{\boldsymbol{q}},\ddot{\boldsymbol{q}} \in \mathbb{R}^n$ describe the link-side positions, velocities, and accelerations, respectively. Analogously, the quantities $\boldsymbol{\theta}_1,\dot{\boldsymbol{\theta}}_1,\ddot{\boldsymbol{\theta}}_1 \in \mathbb{R}^n$ and $\boldsymbol{\theta}_2,\dot{\boldsymbol{\theta}}_2,\ddot{\boldsymbol{\theta}}_2 \in \mathbb{R}^n$ represent the corresponding variables of the two motors. The deflection $\boldsymbol{\varphi}_i^\theta$ for $i = 1,2$ is defined as $\boldsymbol{\theta}_i - \boldsymbol{q}$. Consequently, the link-side dynamics are given by (1) and the motor-side dynamics by (2)–(3). They are coupled through the elastic elements with generalized elastic forces $\boldsymbol{\tau}_1(\boldsymbol{\varphi}_1^\theta)$, $\boldsymbol{\tau}_2(\boldsymbol{\varphi}_2^\theta) \in \mathbb{R}^n$. The components of $\boldsymbol{\tau}_1$ and $\boldsymbol{\tau}_2$ are assumed to be strictly monotonic increasing functions and at least two times continuously differentiable. The symmetric and positive definite link inertia matrix is denoted by $\boldsymbol{M}(\boldsymbol{q}) \in \mathbb{R}^{n\times n}$, with singular values bounded above and below away from zero [20] such that $\boldsymbol{M}^{-1}(\boldsymbol{q})$ exists and is bounded as well. The Coriolis and centrifugal matrix $\boldsymbol{C}(\boldsymbol{q},\dot{\boldsymbol{q}}) \in \mathbb{R}^{n\times n}$ is formulated such that $\dot{\boldsymbol{M}}(\boldsymbol{q},\dot{\boldsymbol{q}}) = \boldsymbol{C}(\boldsymbol{q},\dot{\boldsymbol{q}}) + \boldsymbol{C}(\boldsymbol{q},\dot{\boldsymbol{q}})^T$ holds [21]. Gravitational forces are represented by $\boldsymbol{g}(\boldsymbol{q}) \in \mathbb{R}^n$. The diagonal matrices of the constant, symmetric, and positive definite motor inertias reflected on the link-side are described by $\boldsymbol{B}_1,\boldsymbol{B}_2 \in \mathbb{R}^{n\times n}$. The control inputs on the motor side are $\boldsymbol{u}_1,\boldsymbol{u}_2 \in \mathbb{R}^n$.

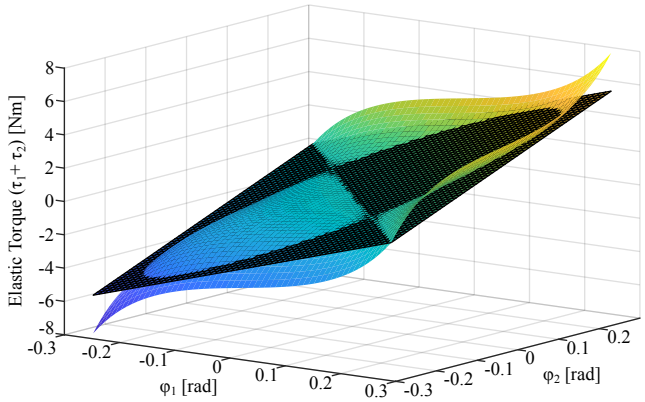

Fig. 2. Visualization of the approximation of the nonlinear elastic torque function (colored) of the BAVS integrated in the forearm rotation of the DLR robot *David* by a linear function (black).

In [7] a control method for compliantly actuated robots was proposed that implements link-side motion tracking and injects a desired link-side damping. The main features of the approach are the preservation of the link-side inertial properties and of the elastic structure of the original plant dynamics [7]. Inspired by that, this work aims at a controller that achieves link-side tracking and damping injection, while simultaneously regulating the pretension of the elastic element to a desired value. To ease the stability proof in Section IV, the inherent nonlinear elastic characteristics $\boldsymbol{\tau}_i(\boldsymbol{\varphi}_i^\theta)$ are replaced by linear ones, yet, in the sense of [7], changing the elastic structure as little as possible.

Each line of $\boldsymbol{\tau}_i(\boldsymbol{\varphi}_i^\theta)$ in (1)-(3) represents a nonlinear function of the deflection $\boldsymbol{\varphi}_i^\theta$. This nonlinear function is approximated by a linear one using a least squares fitting. This procedure is visualized in Fig. 2 exemplary for the nonlinear elastic elements how they are integrated in the forearm rotation of the DLR robot *David*. The slope of the fitted function delivers the constant stiffnesses K_1 and K_2, that form the diagonal entries of $\boldsymbol{K}_1,\boldsymbol{K}_2 \in \mathbb{R}^{n\times n}$.

Inspired by [22], we aim for the following closed-loop dynamics

$$\boldsymbol{M}\ddot{\tilde{\boldsymbol{q}}} + (\boldsymbol{C}+\boldsymbol{D}_q)\dot{\tilde{\boldsymbol{q}}} + \boldsymbol{K}_q\tilde{\boldsymbol{q}} = \boldsymbol{K}_1\boldsymbol{\varphi}_1 + \boldsymbol{K}_2\boldsymbol{\varphi}_2 + \boldsymbol{\tau}_{\text{ext}} \tag{4}$$

$$\boldsymbol{B}_1\ddot{\boldsymbol{\eta}}_1 + \boldsymbol{K}_1\boldsymbol{\varphi}_1 = \boldsymbol{\tau}_{0,1} - \boldsymbol{D}_{\eta,1}\dot{\boldsymbol{\eta}}_1 \tag{5}$$

$$\boldsymbol{B}_2\ddot{\boldsymbol{\eta}}_2 + \boldsymbol{K}_2\boldsymbol{\varphi}_2 = \boldsymbol{\tau}_{0,2} - \boldsymbol{D}_{\eta,2}\dot{\boldsymbol{\eta}}_2 \tag{6}$$

The link-side tracking error is defined by $\tilde{\boldsymbol{q}} = \boldsymbol{q} - \boldsymbol{q}_\mathrm{d}(t) \in \mathbb{R}^n$ with the desired link-side trajectory $\boldsymbol{q}_\mathrm{d}(t) \in \mathcal{C}^4$ and $\|\boldsymbol{q}_\mathrm{d}\|, \|\dot{\boldsymbol{q}}_\mathrm{d}\|, \ldots, \|\boldsymbol{q}_\mathrm{d}^{(4)}\|$ being bounded. In (4)-(6) the desired closed-loop dynamics are introduced in new motor coordinates $\boldsymbol{\eta}_1, \boldsymbol{\eta}_2 \in \mathbb{R}^n$, which can be interpreted as virtual motor coordinates, that reflect the desired link-side behavior to the motor side. The virtual motor velocities and accelerations are denoted by $\dot{\boldsymbol{\eta}}_1, \dot{\boldsymbol{\eta}}_2 \in \mathbb{R}^n$ and $\ddot{\boldsymbol{\eta}}_1, \ddot{\boldsymbol{\eta}}_2 \in \mathbb{R}^n$, respectively. The virtual deflection $\boldsymbol{\varphi}_i = \boldsymbol{\eta}_i - \tilde{\boldsymbol{q}} \in \mathbb{R}^n$ for $i = 1, 2$ is introduced. The damping matrices $\boldsymbol{D}_q, \boldsymbol{D}_{\eta,1}, \boldsymbol{D}_{\eta,2} \in \mathbb{R}^{n\times n}$ are symmetric, positive definite and bounded. The constant, diagonal, positive definite proportional gain matrix on the tracking error is represented by $\boldsymbol{K}_q \in \mathbb{R}^{n\times n}$. The vectors $\boldsymbol{\tau}_{0,1}, \boldsymbol{\tau}_{0,2} \in \mathbb{R}^n$ describe internal torques and are chosen such that $\boldsymbol{\tau}_{0,1} + \boldsymbol{\tau}_{0,2} = \boldsymbol{0}$ holds.

B. Coordinate Transformation

Comparison of (1) and (4) yield

$$\boldsymbol{\tau}_1(\boldsymbol{\varphi}_1^\theta) + \boldsymbol{\tau}_2(\boldsymbol{\varphi}_2^\theta) = \boldsymbol{K}_1\boldsymbol{\varphi}_1 + \boldsymbol{K}_2\boldsymbol{\varphi}_2 + \boldsymbol{\tau}_\mathrm{d} \tag{7}$$

with

$$\boldsymbol{\tau}_\mathrm{d} = \boldsymbol{g} + \boldsymbol{M}(\boldsymbol{q})\ddot{\boldsymbol{q}}_\mathrm{d} + \boldsymbol{C}(\boldsymbol{q}, \dot{\boldsymbol{q}})\dot{\boldsymbol{q}}_\mathrm{d} - \boldsymbol{D}_q\dot{\tilde{\boldsymbol{q}}} - \boldsymbol{K}_q\tilde{\boldsymbol{q}}. \tag{8}$$

Motivated by [17], we impose a constraint that the pretension is equal in the original and in the virtual coordinates:

$$\boldsymbol{\tau}_1(\boldsymbol{\varphi}_1^\theta) - \boldsymbol{\tau}_2(\boldsymbol{\varphi}_2^\theta) = \boldsymbol{K}_1\boldsymbol{\varphi}_1 - \boldsymbol{K}_2\boldsymbol{\varphi}_2. \tag{9}$$

Here the difference of the elastic torques is referred to as pretension of the mechanism. With (7) and (9) the transformation from $\boldsymbol{\theta}_i$ to $\boldsymbol{\eta}_i$ for $i = 1, 2$ is uniquely determined:

$$\begin{pmatrix}\boldsymbol{\varphi}_1\\ \boldsymbol{\varphi}_2\end{pmatrix} = \begin{pmatrix}\boldsymbol{K}_1 & \boldsymbol{K}_2\\ \boldsymbol{K}_1 & -\boldsymbol{K}_2\end{pmatrix}^{-1}\begin{pmatrix}\boldsymbol{\tau}_1(\boldsymbol{\varphi}_1^\theta) + \boldsymbol{\tau}_2(\boldsymbol{\varphi}_2^\theta) - \boldsymbol{\tau}_\mathrm{d}\\ \boldsymbol{\tau}_1(\boldsymbol{\varphi}_1^\theta) - \boldsymbol{\tau}_2(\boldsymbol{\varphi}_2^\theta)\end{pmatrix} \tag{10}$$

C. Control Law

Consequently, the time derivative of (10) yields

$$\boldsymbol{H}\begin{pmatrix}\dot{\boldsymbol{\varphi}}_1^\theta\\ \dot{\boldsymbol{\varphi}}_2^\theta\end{pmatrix} = \boldsymbol{K}\begin{pmatrix}\dot{\boldsymbol{\varphi}}_1\\ \dot{\boldsymbol{\varphi}}_2\end{pmatrix} + \begin{pmatrix}\dot{\boldsymbol{\tau}}_\mathrm{d}\\ \boldsymbol{0}\end{pmatrix} \tag{11}$$

with

$$\boldsymbol{H} = \begin{pmatrix}\boldsymbol{\kappa}_1(\boldsymbol{\varphi}_1^\theta) & \boldsymbol{\kappa}_2(\boldsymbol{\varphi}_2^\theta)\\ \boldsymbol{\kappa}_1(\boldsymbol{\varphi}_1^\theta) & -\boldsymbol{\kappa}_2(\boldsymbol{\varphi}_2^\theta)\end{pmatrix}, \tag{12}$$

$$\boldsymbol{K} = \begin{pmatrix}\boldsymbol{K}_1 & \boldsymbol{K}_2\\ \boldsymbol{K}_1 & -\boldsymbol{K}_2\end{pmatrix}. \tag{13}$$

Where the terms $\boldsymbol{\kappa}_i(\boldsymbol{\varphi}_i^\theta)$ for $i = 1, 2$ describe the derivative of the generalized elastic forces $\boldsymbol{\tau}_i(\boldsymbol{\varphi}_i^\theta)$ with respect to the argument $\boldsymbol{\varphi}_i^\theta$. After differentiating (11) with respect to time, the motor accelerations can be represented as

$$\begin{aligned}\begin{pmatrix}\ddot{\boldsymbol{\theta}}_1\\ \ddot{\boldsymbol{\theta}}_2\end{pmatrix} &= \boldsymbol{H}^{-1}\boldsymbol{K}\begin{pmatrix}\ddot{\boldsymbol{\varphi}}_1\\ \ddot{\boldsymbol{\varphi}}_2\end{pmatrix} + \boldsymbol{H}^{-1}\begin{pmatrix}\ddot{\boldsymbol{\tau}}_\mathrm{d}\\ \boldsymbol{0}\end{pmatrix} + \begin{pmatrix}\ddot{\boldsymbol{q}}\\ \ddot{\boldsymbol{q}}\end{pmatrix}\\ &\quad -\boldsymbol{H}^{-1}\dot{\boldsymbol{H}}\Big(\boldsymbol{H}^{-1}\boldsymbol{K}\begin{pmatrix}\dot{\boldsymbol{\varphi}}_1\\ \dot{\boldsymbol{\varphi}}_2\end{pmatrix} + \boldsymbol{H}^{-1}\begin{pmatrix}\dot{\boldsymbol{\tau}}_\mathrm{d}\\ \boldsymbol{0}\end{pmatrix}\Big).\end{aligned} \tag{14}$$

Transforming (2)–(3) into the new motor coordinates yields

$$\boldsymbol{B}\boldsymbol{H}^{-1}\boldsymbol{K}\begin{pmatrix}\ddot{\boldsymbol{\eta}}_1\\ \ddot{\boldsymbol{\eta}}_2\end{pmatrix} + \boldsymbol{B}\boldsymbol{b} + \begin{pmatrix}\boldsymbol{\tau}_1(\boldsymbol{\varphi}_1^\theta)\\ \boldsymbol{\tau}_2(\boldsymbol{\varphi}_2^\theta)\end{pmatrix} = \begin{pmatrix}\boldsymbol{u}_1\\ \boldsymbol{u}_2\end{pmatrix} \tag{15}$$

with

$$\boldsymbol{B} = \begin{pmatrix}\boldsymbol{B}_1 & \boldsymbol{0}\\ \boldsymbol{0} & \boldsymbol{B}_2\end{pmatrix}, \tag{16}$$

$$\boldsymbol{b} = \begin{pmatrix}\ddot{\boldsymbol{q}}\\ \ddot{\boldsymbol{q}}\end{pmatrix} + \boldsymbol{H}^{-1}\left(\begin{pmatrix}\ddot{\boldsymbol{\tau}}_\mathrm{d}\\ \boldsymbol{0}\end{pmatrix} - \boldsymbol{K}\begin{pmatrix}\ddot{\tilde{\boldsymbol{q}}}\\ \ddot{\tilde{\boldsymbol{q}}}\end{pmatrix} - \dot{\boldsymbol{H}}\begin{pmatrix}\dot{\boldsymbol{\varphi}}_1^\theta\\ \dot{\boldsymbol{\varphi}}_2^\theta\end{pmatrix}\right). \tag{17}$$

By choosing the control law as

$$\boldsymbol{u} = \boldsymbol{B}\boldsymbol{b} + \begin{pmatrix}\boldsymbol{\tau}_1(\boldsymbol{\varphi}_1^\theta)\\ \boldsymbol{\tau}_2(\boldsymbol{\varphi}_2^\theta)\end{pmatrix} - \boldsymbol{B}\boldsymbol{H}^{-1}\boldsymbol{K}\boldsymbol{B}^{-1}\left(\begin{pmatrix}\boldsymbol{K}_1\boldsymbol{\varphi}_1\\ \boldsymbol{K}_2\boldsymbol{\varphi}_2\end{pmatrix} - \bar{\boldsymbol{u}}\right) \tag{18}$$

with

$$\bar{\boldsymbol{u}} = \begin{pmatrix}\boldsymbol{\tau}_{0,1} - \boldsymbol{D}_{\eta,1}\dot{\boldsymbol{\eta}}_1\\ \boldsymbol{\tau}_{0,2} - \boldsymbol{D}_{\eta,2}\dot{\boldsymbol{\eta}}_2\end{pmatrix} \tag{19}$$

one straightforwardly obtains (5)–(6).

D. Shift Equilibrium Point to Origin

The system state vector of (4)-(6) is defined as

$$\boldsymbol{z} = \begin{bmatrix}\tilde{\boldsymbol{q}}^T & \boldsymbol{\eta}_1^T & \boldsymbol{\eta}_2^T & \dot{\tilde{\boldsymbol{q}}}^T & \dot{\boldsymbol{\eta}}_1^T & \dot{\boldsymbol{\eta}}_2^T\end{bmatrix}^T. \tag{20}$$

For $\boldsymbol{\tau}_\mathrm{ext} = 0$ the unique equilibrium point of the closed-loop system is given by

$$\boldsymbol{z}_\mathrm{eq} = \begin{bmatrix}\boldsymbol{0}^T & (\boldsymbol{K}_1^{-1}\boldsymbol{\tau}_{0,1})^T & (\boldsymbol{K}_2^{-1}\boldsymbol{\tau}_{0,2})^T & \boldsymbol{0}^T & \boldsymbol{0}^T & \boldsymbol{0}^T\end{bmatrix}^T \tag{21}$$

For the following stability analysis the system equilibrium is shifted to the origin. To achieve this, new coordinates $\tilde{\boldsymbol{\eta}}_1$ and $\tilde{\boldsymbol{\eta}}_2$ are introduced as

$$\begin{bmatrix}\tilde{\boldsymbol{\eta}}_1\\ \tilde{\boldsymbol{\eta}}_2\end{bmatrix} = \begin{bmatrix}\boldsymbol{\eta}_1\\ \boldsymbol{\eta}_2\end{bmatrix} - \begin{bmatrix}\boldsymbol{K}_1^{-1}\boldsymbol{\tau}_{0,1}\\ \boldsymbol{K}_2^{-1}\boldsymbol{\tau}_{0,2}\end{bmatrix}. \tag{22}$$

Using these shifted coordinates we define a new system state vector $\boldsymbol{x}$ as

$$\boldsymbol{x} = \begin{bmatrix}\tilde{\boldsymbol{q}}^T & \tilde{\boldsymbol{\eta}}_1^T & \tilde{\boldsymbol{\eta}}_2^T & \dot{\tilde{\boldsymbol{q}}}^T & \dot{\tilde{\boldsymbol{\eta}}}_1^T & \dot{\tilde{\boldsymbol{\eta}}}_2^T\end{bmatrix}^T. \tag{23}$$

For the following passivity and stability analysis, it is assumed that the pretension is constant, thus $\ddot{\boldsymbol{\tau}}_{0,i} = \dot{\boldsymbol{\tau}}_{0,i} = \boldsymbol{0}$. With this assumption, the resulting system dynamics can be expressed as

$$\boldsymbol{M}\ddot{\tilde{\boldsymbol{q}}} + (\boldsymbol{C} + \boldsymbol{D}_q)\dot{\tilde{\boldsymbol{q}}} + \boldsymbol{K}_q\tilde{\boldsymbol{q}} = \boldsymbol{K}_1\tilde{\boldsymbol{\varphi}}_1 + \boldsymbol{K}_2\tilde{\boldsymbol{\varphi}}_2 + \boldsymbol{\tau}_\mathrm{ext}, \tag{24}$$

$$\boldsymbol{B}_1\ddot{\tilde{\boldsymbol{\eta}}}_1 + \boldsymbol{K}_1\tilde{\boldsymbol{\varphi}}_1 = -\boldsymbol{D}_{\eta,1}\dot{\tilde{\boldsymbol{\eta}}}_1, \tag{25}$$

$$\boldsymbol{B}_2\ddot{\tilde{\boldsymbol{\eta}}}_2 + \boldsymbol{K}_2\tilde{\boldsymbol{\varphi}}_2 = -\boldsymbol{D}_{\eta,2}\dot{\tilde{\boldsymbol{\eta}}}_2. \tag{26}$$

Analogously to $\boldsymbol{\varphi}_i$, $\tilde{\boldsymbol{\varphi}}_i = \tilde{\boldsymbol{\eta}}_i - \tilde{\boldsymbol{q}}$ for $i = 1, 2$ is introduced.

III. Passivity Analysis

In this section we analyze the passivity property of the closed-loop system, that is $\dot{S} \leq \dot{\tilde{\boldsymbol{q}}}^T \boldsymbol{\tau}_{\text{ext}}$. As a non-negative storage function we choose

$$S_{\tilde{q}} := \frac{1}{2}\dot{\tilde{\boldsymbol{q}}}^T \boldsymbol{M} \dot{\tilde{\boldsymbol{q}}} + \frac{1}{2}\tilde{\boldsymbol{q}}^T \boldsymbol{K}_q \tilde{\boldsymbol{q}} \tag{27}$$

for the closed-loop link-side dynamics and the non-negative function

$$\begin{aligned} S_{\tilde{\eta}} := &\frac{1}{2}\dot{\tilde{\boldsymbol{\eta}}}_1^T \boldsymbol{B}_1 \dot{\tilde{\boldsymbol{\eta}}}_1 + \frac{1}{2}\tilde{\boldsymbol{\varphi}}_1^T \boldsymbol{K}_1 \tilde{\boldsymbol{\varphi}}_1 \\ &+ \frac{1}{2}\dot{\tilde{\boldsymbol{\eta}}}_2^T \boldsymbol{B}_2 \dot{\tilde{\boldsymbol{\eta}}}_2 + \frac{1}{2}\tilde{\boldsymbol{\varphi}}_2^T \boldsymbol{K}_2 \tilde{\boldsymbol{\varphi}}_2 \end{aligned} \tag{28}$$

for the motor dynamics. For analysis, the storage functions are derived once with respect to time and evaluated along the solutions of (24)-(26) and we get

$$\dot{S}_{\tilde{q}} = \dot{\tilde{\boldsymbol{q}}}^T \boldsymbol{\tau}_{\text{ext}} - \dot{\tilde{\boldsymbol{q}}}^T \boldsymbol{D}_q \dot{\tilde{\boldsymbol{q}}} + \dot{\tilde{\boldsymbol{q}}}^T \boldsymbol{K}_1 \tilde{\boldsymbol{\varphi}}_1 + \dot{\tilde{\boldsymbol{q}}}^T \boldsymbol{K}_2 \tilde{\boldsymbol{\varphi}}_2, \tag{29}$$

$$\dot{S}_{\tilde{\eta}} = -\dot{\tilde{\boldsymbol{\eta}}}_1^T \boldsymbol{D}_{\eta,1} \dot{\tilde{\boldsymbol{\eta}}}_1 - \dot{\tilde{\boldsymbol{\eta}}}_2^T \boldsymbol{D}_{\eta,2} \dot{\tilde{\boldsymbol{\eta}}}_2 - \dot{\tilde{\boldsymbol{q}}}^T \boldsymbol{K}_1 \tilde{\boldsymbol{\varphi}}_1 - \dot{\tilde{\boldsymbol{q}}}^T \boldsymbol{K}_2 \tilde{\boldsymbol{\varphi}}_2. \tag{30}$$

Proposition 1. *The closed-loop system* (24)-(26) *represents a passive map from the external force $\boldsymbol{\tau}_{\text{ext}}$ to the velocities of the link-side tracking error $\dot{\tilde{\boldsymbol{q}}}$.*

Proof. Consider the total, non-negative storage function $S_{\text{tot}} = S_{\tilde{q}} + S_{\tilde{\eta}}$ combining (27) and (28). Its time derivative is given by the sum of (29) and (30)

$$\dot{\tilde{\boldsymbol{q}}}^T \boldsymbol{\tau}_{\text{ext}} - \dot{\tilde{\boldsymbol{q}}}^T \boldsymbol{D}_q \dot{\tilde{\boldsymbol{q}}} - \dot{\tilde{\boldsymbol{\eta}}}_1^T \boldsymbol{D}_{\eta,1} \dot{\tilde{\boldsymbol{\eta}}}_1 - \dot{\tilde{\boldsymbol{\eta}}}_2^T \boldsymbol{D}_{\eta,2} \dot{\tilde{\boldsymbol{\eta}}}_2 \leq \dot{\tilde{\boldsymbol{q}}}^T \boldsymbol{\tau}_{\text{ext}}, \tag{31}$$

which completes the proof. □

Remark 1. *Note that in case of regulation control, the simplification $\dot{\tilde{\boldsymbol{q}}} = \dot{\boldsymbol{q}}$ holds. Consequently, with* (31) *one can show passivity of the controlled robot for the input $\boldsymbol{\tau}_{\text{ext}}$, the output $\dot{\boldsymbol{q}}$, and the storage function S_{tot}. Since $\dot{\boldsymbol{q}}^T \boldsymbol{\tau}_{\text{ext}}$ represents the natural power port for physical interaction, this conclusion of passivity is of high relevance in practice.*

IV. Stability analysis

In this section the stability properties of the time-variant closed-loop dynamics (24)-(26) for $\boldsymbol{\tau}_{\text{ext}} = \boldsymbol{0}$ are analyzed.

Proposition 2. *The origin of the closed-loop system* (24)-(26)*, in absence of external forces $\boldsymbol{\tau}_{\text{ext}}$, is uniformly asymptotically stable.*

The closed-loop dynamics (24)-(26) can be written as

$$\dot{\boldsymbol{x}} = \boldsymbol{f}(t, \boldsymbol{x}) \tag{32}$$

with state $\boldsymbol{x} \in \mathbb{R}^{6n}$. $\boldsymbol{f}$ is a continuous function $\boldsymbol{f} : I \times \Omega \to \mathbb{R}^{6n}$, with $I = [t_0, \infty)$ for some $t_0 \in \mathbb{R}$ and Ω is a bounded set in $\mathbb{R}^{6n}$, containing the origin. We know that the origin is an equilibrium point of (32). To show uniform asymptotic stability of the non-autonomous system (24)-(26) we use Lyapunov theory and Matrosov's theorem. The latter was first introduced in [23]. It states:

Theorem 1. *[24] Let there exist two $\mathcal{C}^1$ functions $V : I \times \Omega \to \mathbb{R}$, $W : I \times \Omega \to \mathbb{R}$, a $\mathcal{C}^0$ function $V^* : \Omega \to \mathbb{R}$, three functions $a, b, c \in \mathcal{K}$ and two constants $S > 0$ and $T > 0$ such that, for every $(t, \boldsymbol{x}) \in I \times \Omega$*

(i) $a(\|\boldsymbol{x}\|) \leq V(t, \boldsymbol{x}) \leq b(\|\boldsymbol{x}\|)$;
(ii) $\dot{V}(t, \boldsymbol{x}) \leq V^*(\boldsymbol{x}) \leq 0; E := \{\boldsymbol{x} \in \Omega : V^*(\boldsymbol{x}) = 0\}$;
(iii) $|W(t, \boldsymbol{x})| < S$;
(iv) $\max(d(\boldsymbol{x}, E), |\dot{W}(t, \boldsymbol{x})|) \geq c(\|\boldsymbol{x}\|)$[1];
(v) $\|\boldsymbol{f}(t, \boldsymbol{x})\| < T$;

choosing $\alpha > 0$ such that $\bar{B}_\alpha \subset \Omega$, let us put for every $t \in I$

$$V_{t,\alpha}^{-1} = \boldsymbol{x} \in \Omega : V(t, \boldsymbol{x}) \leq a(\alpha). \tag{33}$$

Then

(i) *for any $t_0 \in I$ and any $\boldsymbol{x}_0 \in V_{t_0,\alpha}^{-1}$, any solution $\boldsymbol{x}(t)$ of* (32)*, passing through $(t_0, \boldsymbol{x}_0) \in I \times \Omega$, tends to zero uniformly in t_0 and $\boldsymbol{x}_0$, when $t \to \infty$.*
(ii) *the origin is uniformly asymptotically stable.*

As time-variant, Lyapunov function candiate $V : [0, \infty) \times \Omega \to \mathbb{R}$ we choose

$$V(t, \boldsymbol{x}) = S_{\tilde{q}}(t, \boldsymbol{x}) + S_{\tilde{\eta}}(t, \boldsymbol{x}) = \frac{1}{2}\boldsymbol{x}^T \underbrace{\begin{bmatrix} \boldsymbol{P} & \boldsymbol{0} \\ \boldsymbol{0} & \boldsymbol{Q} \end{bmatrix}}_{\boldsymbol{R}} \boldsymbol{x} \tag{34}$$

where

$$\boldsymbol{P} = \begin{bmatrix} \boldsymbol{K}_q + \boldsymbol{K}_1 + \boldsymbol{K}_2 & -\boldsymbol{K}_1 & -\boldsymbol{K}_2 \\ -\boldsymbol{K}_1 & \boldsymbol{K}_1 & \boldsymbol{0} \\ -\boldsymbol{K}_2 & \boldsymbol{0} & \boldsymbol{K}_2 \end{bmatrix}, \tag{35}$$

$$\boldsymbol{Q} = \text{diag}(\boldsymbol{M}, \boldsymbol{B}_1, \boldsymbol{B}_2). \tag{36}$$

By applying the Schur-complement-condition, one can show, that $V(t, \boldsymbol{x})$ is positive definite.
From (31) it results

$$\dot{V}(t, \boldsymbol{x}) = -\dot{\tilde{\boldsymbol{q}}}^T \boldsymbol{D}_q \dot{\tilde{\boldsymbol{q}}} - \dot{\tilde{\boldsymbol{\eta}}}_1^T \boldsymbol{D}_{\eta,1} \dot{\tilde{\boldsymbol{\eta}}}_1 - \dot{\tilde{\boldsymbol{\eta}}}_2^T \boldsymbol{D}_{\eta,2} \dot{\tilde{\boldsymbol{\eta}}}_2 \tag{37}$$

which is negative semi-definite, since $\boldsymbol{D}_q$, $\boldsymbol{D}_{\eta,1}$ and $\boldsymbol{D}_{\eta,2}$ are positive definite (4)-(6).

Condition (i): Due to the fact that $\boldsymbol{R}$ (34) is symmetric and positive definite, one can directly find class $\mathcal{K}$ functions a, b that form lower and upper bounds for V as

$$a(\|\boldsymbol{x}\|) = \frac{1}{2}\underline{\lambda}(\boldsymbol{R})\|\boldsymbol{x}\|^2 \quad \text{and} \quad b(\|\boldsymbol{x}\|) = \frac{1}{2}\bar{\lambda}(\boldsymbol{R})\|\boldsymbol{x}\|^2, \tag{38}$$

where $\underline{\lambda}(\boldsymbol{R})$ and $\bar{\lambda}(\boldsymbol{R})$ denote the minimum and maximum eigenvalue of $\boldsymbol{R}$, respectively.

Condition (ii): We choose $V^*(\boldsymbol{x}) = \dot{V}(t, \boldsymbol{x})$. According to (37) the problematic set E, where $V^*(\boldsymbol{x}) = 0$ is then given by $E = \{\boldsymbol{x} \in \Omega : \dot{\tilde{\boldsymbol{q}}} = \dot{\tilde{\boldsymbol{\eta}}}_1 = \dot{\tilde{\boldsymbol{\eta}}}_2 = \boldsymbol{0}\}$.

Condition (iii): We define the auxiliary function $W : [0, \infty) \times \Omega \to \mathbb{R}$ as

$$W(t, \boldsymbol{x}) := \ddot{V}(t, \boldsymbol{x}). \tag{39}$$

Condition (iii) is fulfilled, if $|W(t, \boldsymbol{x})|$ is bounded. We get

$$W(t, \boldsymbol{x}) = -2(\dot{\tilde{\boldsymbol{q}}}^T \boldsymbol{D}_q \ddot{\tilde{\boldsymbol{q}}} + \dot{\tilde{\boldsymbol{\eta}}}_1^T \boldsymbol{D}_{\eta,1} \ddot{\tilde{\boldsymbol{\eta}}}_1 + \dot{\tilde{\boldsymbol{\eta}}}_2^T \boldsymbol{D}_{\eta,2} \ddot{\tilde{\boldsymbol{\eta}}}_2). \tag{40}$$

Since $V(t, \boldsymbol{x})$ is positive definite and $\dot{V}(t, \boldsymbol{x})$ is negative semi-definite, the system (24)-(26) is uniformly stable. Thus, for the arbitrarily large but bounded set Ω the state vector $\boldsymbol{x}(t)$ is

[1] $d(\boldsymbol{x}, E)$ denotes the minimum distance of point $\boldsymbol{x}$ to set E

bounded $\forall t \in [t_0, \infty)$ for any starting condition $\boldsymbol{x}_0 \in \Omega$. As $\boldsymbol{x}$ is bounded and $\boldsymbol{D}_q$, $\boldsymbol{D}_{\eta,1}$ and $\boldsymbol{D}_{\eta,2}$ are bounded as well, one can see, that apart from $\ddot{\tilde{\boldsymbol{q}}}$, $\ddot{\tilde{\boldsymbol{\eta}}}_1$ and $\ddot{\tilde{\boldsymbol{\eta}}}_2$, all terms on the RHS of (40) are bounded. To show the boundedness of these terms, (24)-(26) are solved for the second time derivatives with $\boldsymbol{\tau}_{\text{ext}} = \boldsymbol{0}$. We know that $\boldsymbol{M}^{-1}$, $\boldsymbol{B}_1^{-1}$ and $\boldsymbol{B}_2^{-1}$ exist and are bounded (1), moreover $\boldsymbol{C}\dot{\tilde{\boldsymbol{q}}}$ is bounded for bounded $\dot{\tilde{\boldsymbol{q}}}$. Since in (24)-(26) $\boldsymbol{K}_q, \boldsymbol{K}_1$ and $\boldsymbol{K}_2$ are bounded too, it follows that $\ddot{\tilde{\boldsymbol{q}}}$, $\ddot{\tilde{\boldsymbol{\eta}}}_1, \ddot{\tilde{\boldsymbol{\eta}}}_2$ and thus $|W(t, \boldsymbol{x})|$ are bounded.

To show that condition (iv) of Matrosov's theorem is fulfilled, one can use the following lemma from [25]. For the corresponding proof see [25].

Lemma 1. *[25] Condition (iv) of Matrosov's theorem is satisfied if conditions below are satisfied.*

(iv.a) *$\dot{W}(t, \boldsymbol{x})$ is continuous in both arguments and depends on time in the following way. $\dot{W}(t, \boldsymbol{x}) = g(\beta(t), \boldsymbol{x})$ where g is continuous in both of its arguments. $\beta(t)$ is also continuous and its image lies in a bounded set. (For simplicity, we simply say that $\dot{W}(t, \boldsymbol{x})$ depends on time continuously through a bounded function.)*

(iv.b) *There exists a class $\mathcal{K}$ function, k, such that $|\dot{W}(t, \boldsymbol{x})| \geq k(\|\boldsymbol{x}\|) \forall \boldsymbol{x} \in E$ and $t \geq t_0$.*

Condition (iv): To verify condition (iv.a), $\dot{W}(t, \boldsymbol{x})$ has to depend continuously on $\boldsymbol{x}$ and continuously on time t through a bounded function. The time derivative $\dot{W}(t, \boldsymbol{x})$ is given by the following expression:

$$\begin{aligned}\dot{W}(t, \boldsymbol{x}) = -2(&\ddot{\tilde{\boldsymbol{q}}}^T \boldsymbol{D}_q \ddot{\tilde{\boldsymbol{q}}} + \dot{\tilde{\boldsymbol{q}}}^T \boldsymbol{D}_q \tilde{\boldsymbol{q}}^{(3)} + \ddot{\tilde{\boldsymbol{\eta}}}_1^T \boldsymbol{D}_{\eta,1} \ddot{\tilde{\boldsymbol{\eta}}}_1 \\ &+ \dot{\tilde{\boldsymbol{\eta}}}_1^T \boldsymbol{D}_{\eta,1} \tilde{\boldsymbol{\eta}}_1^{(3)} + \ddot{\tilde{\boldsymbol{\eta}}}_2^T \boldsymbol{D}_{\eta,2} \ddot{\tilde{\boldsymbol{\eta}}}_2 + \dot{\tilde{\boldsymbol{\eta}}}_2^T \boldsymbol{D}_{\eta,2} \tilde{\boldsymbol{\eta}}_2^{(3)}).\end{aligned} \tag{41}$$

Using (24)-(26) one can see that $\ddot{\tilde{\boldsymbol{q}}}$ is continuous in $\tilde{\boldsymbol{q}}$, $\dot{\tilde{\boldsymbol{q}}}$, $\tilde{\boldsymbol{\eta}}_1$, $\tilde{\boldsymbol{\eta}}_2$ and in time through the bounded functions $\boldsymbol{q}_{\text{d}}(t), \dot{\boldsymbol{q}}_{\text{d}}(t), \ddot{\boldsymbol{q}}_{\text{d}}(t)$. $\ddot{\tilde{\boldsymbol{\eta}}}_1$ is continuous in $\tilde{\boldsymbol{q}}$, $\dot{\tilde{\boldsymbol{q}}}$, $\tilde{\boldsymbol{\eta}}_1$, $\dot{\tilde{\boldsymbol{\eta}}}_1$ and $\ddot{\tilde{\boldsymbol{\eta}}}_2$ is continuous in $\tilde{\boldsymbol{q}}$, $\dot{\tilde{\boldsymbol{q}}}$, $\tilde{\boldsymbol{\eta}}_2$, $\dot{\tilde{\boldsymbol{\eta}}}_2$. Both are continuous in time through the bounded functions $\boldsymbol{q}_{\text{d}}(t), \dot{\boldsymbol{q}}_{\text{d}}(t), \ddot{\boldsymbol{q}}_{\text{d}}(t), \boldsymbol{q}_{\text{d}}^{(3)}(t)$. To show that the third derivatives of $\tilde{\boldsymbol{q}}$,$\tilde{\boldsymbol{\eta}}_1$ and $\tilde{\boldsymbol{\eta}}_2$ are continously in $\boldsymbol{x}$ and depend continuously on time through a bounded function, (24)-(26) are differentiated with respect to time:

$$\begin{aligned}\tilde{\boldsymbol{q}}^{(3)} = \boldsymbol{M}^{-1}\Big(&\boldsymbol{K}_1 \dot{\tilde{\boldsymbol{\varphi}}}_1 + \boldsymbol{K}_2 \dot{\tilde{\boldsymbol{\varphi}}}_2 - \dot{\boldsymbol{M}} \ddot{\tilde{\boldsymbol{q}}} - \dot{\boldsymbol{C}} \dot{\tilde{\boldsymbol{q}}} \\ &- (\boldsymbol{C} - \boldsymbol{D}_q) \ddot{\tilde{\boldsymbol{q}}} - \boldsymbol{K}_q \dot{\tilde{\boldsymbol{q}}}\Big)\end{aligned} \tag{42}$$

$$\tilde{\boldsymbol{\eta}}_1^{(3)} = \boldsymbol{B}_1^{-1}(-\boldsymbol{K}_1 \dot{\tilde{\boldsymbol{\varphi}}}_1 - \boldsymbol{D}_{\eta,1} \ddot{\tilde{\boldsymbol{\eta}}}_1) \tag{43}$$

$$\tilde{\boldsymbol{\eta}}_2^{(3)} = \boldsymbol{B}_2^{-1}(-\boldsymbol{K}_2 \dot{\tilde{\boldsymbol{\varphi}}}_2 - \boldsymbol{D}_{\eta,2} \ddot{\tilde{\boldsymbol{\eta}}}_2) \tag{44}$$

$\boldsymbol{M}$ is two-times continuously differentiable and $\boldsymbol{M}$ and $\boldsymbol{q}$ are bounded. Thus $\frac{\partial \boldsymbol{M}}{\partial \boldsymbol{q}}$ as well as $\frac{\partial^2 \boldsymbol{M}}{\partial \boldsymbol{q}^2}$ are bounded. From this follows that $\dot{\boldsymbol{M}}$ is bounded. Boundedness of $\ddot{\tilde{\boldsymbol{q}}}$ was already shown in the previous paragraph. Since $\boldsymbol{q}_{\text{d}}(t) \in \mathcal{C}^4$ and $\|\boldsymbol{q}_{\text{d}}\|, \|\dot{\boldsymbol{q}}_{\text{d}}\|, \ldots, \|\boldsymbol{q}_{\text{d}}^{(4)}\|$ are bounded it follows that $\ddot{\boldsymbol{q}}$ is bounded. Thus $\dddot{\boldsymbol{M}}$ is bounded, which is equivalent to the statement that $\dot{\boldsymbol{C}}$ is bounded. It has to be shown that all terms on the RHS of (42)-(44) are bounded, continuous in $\boldsymbol{x}$ and depend continuously on time through bounded functions.

It follows that $\tilde{\boldsymbol{q}}^{(3)}$ exists and depends continuously on $\boldsymbol{x}$ and continuously on time t through the bounded functions $\boldsymbol{q}_{\text{d}}(t)$,$\dot{\boldsymbol{q}}_{\text{d}}(t)$, $\ddot{\boldsymbol{q}}_{\text{d}}(t)$, $\boldsymbol{q}_{\text{d}}^{(3)}(t)$ and $\boldsymbol{q}_{\text{d}}^{(4)}(t)$. To show the same properties for $\tilde{\boldsymbol{\eta}}_1^{(3)}$ and $\tilde{\boldsymbol{\eta}}_2^{(3)}$ one can proceed in an analog fashion, see also [7] for details.

To check condition (iv.b), we evaluate $\dot{W}$ on the critical set E. After substituting the higher derivatives in (41) and evaluation on E we get:

$$\dot{W}(t, \boldsymbol{x}) = -2 \begin{bmatrix} \tilde{\boldsymbol{q}} \\ \tilde{\boldsymbol{\eta}}_1 \\ \tilde{\boldsymbol{\eta}}_2 \end{bmatrix}^T \boldsymbol{A}^T \boldsymbol{\Lambda} \boldsymbol{A} \begin{bmatrix} \tilde{\boldsymbol{q}} \\ \tilde{\boldsymbol{\eta}}_1 \\ \tilde{\boldsymbol{\eta}}_2 \end{bmatrix}, \forall \boldsymbol{x} \in E \tag{45}$$

with

$$\boldsymbol{\Lambda} = \begin{bmatrix} \boldsymbol{\Lambda}_1 & \boldsymbol{0} & \boldsymbol{0} \\ \boldsymbol{0} & \boldsymbol{\Lambda}_2 & \boldsymbol{0} \\ \boldsymbol{0} & \boldsymbol{0} & \boldsymbol{\Lambda}_3 \end{bmatrix} \tag{46}$$

and

$$\boldsymbol{A} = \begin{bmatrix} -\boldsymbol{K}_q - \boldsymbol{K}_1 - \boldsymbol{K}_2 & \boldsymbol{K}_1 & \boldsymbol{K}_2 \\ \boldsymbol{K}_1 & -\boldsymbol{K}_1 & \boldsymbol{0} \\ \boldsymbol{K}_2 & \boldsymbol{0} & -\boldsymbol{K}_2 \end{bmatrix} \tag{47}$$

where

$$\begin{aligned}\boldsymbol{\Lambda}_1 &:= \boldsymbol{M}^{-T} \boldsymbol{D}_q \boldsymbol{M}^{-1} = \boldsymbol{\Lambda}_1^T \\ \boldsymbol{\Lambda}_2 &:= \boldsymbol{B}_1^{-T} \boldsymbol{D}_{\eta,1} \boldsymbol{B}_1^{-1} = \boldsymbol{\Lambda}_2^T \\ \boldsymbol{\Lambda}_3 &:= \boldsymbol{B}_2^{-T} \boldsymbol{D}_{\eta,2} \boldsymbol{B}_2^{-1} = \boldsymbol{\Lambda}_3^T\end{aligned} \tag{48}$$

Since $\boldsymbol{M}^{-1}$ is non-singular and $\boldsymbol{D}_q$ is symmetric and positive definite, following Sylvester's Law of Inertia [26] one can state that $\boldsymbol{\Lambda}_1$ is positive definite. Analogously positive definiteness of $\boldsymbol{\Lambda}_2$ and $\boldsymbol{\Lambda}_3$ can be shown.

The determinant of $\boldsymbol{A}$ results in

$$\det(\boldsymbol{A}) = \prod_{i=1}^{n}(-k_{q,i}) \cdot \prod_{i=1}^{n}(-k_{1,i}) \cdot \prod_{i=1}^{n}(-k_{2,i}) \tag{49}$$

where $k_{q,i}, k_{1,i}, k_{2,i}$ are the diagonal entries of $\boldsymbol{K}_q, \boldsymbol{K}_1, \boldsymbol{K}_2$, respectively. Due to the positive definiteness of $\boldsymbol{K}_q$, $\boldsymbol{K}_1$ and $\boldsymbol{K}_2$ the determinant of $\boldsymbol{A}$ is nonzero. Sylvester's Law of Inertia [26] states that $\boldsymbol{A}^T \boldsymbol{\Lambda} \boldsymbol{A}$ is positive definite.

We can write

$$|\dot{W}(t, \boldsymbol{x})| = 2 \begin{bmatrix} \tilde{\boldsymbol{q}} \\ \tilde{\boldsymbol{\eta}}_1 \\ \tilde{\boldsymbol{\eta}}_2 \end{bmatrix}^T \underbrace{\boldsymbol{A}^T \boldsymbol{\Lambda} \boldsymbol{A}}_{\boldsymbol{\Sigma}} \begin{bmatrix} \tilde{\boldsymbol{q}} \\ \tilde{\boldsymbol{\eta}}_1 \\ \tilde{\boldsymbol{\eta}}_2 \end{bmatrix}, \forall \boldsymbol{x} \in E \tag{50}$$

with $\boldsymbol{\Sigma}$ symmetric and positive definite. Hence

$$k(\|\boldsymbol{x}\|) = 2\underline{\lambda}(\boldsymbol{\Sigma}) \left\| \begin{bmatrix} \tilde{\boldsymbol{q}} \\ \tilde{\boldsymbol{\eta}}_1 \\ \tilde{\boldsymbol{\eta}}_2 \end{bmatrix} \right\|^2, \forall \boldsymbol{x} \in E \tag{51}$$

with $k \in \mathcal{K}$ is a lower bound of $|\dot{W}(t, \boldsymbol{x})|$.

Condition (v): From previous considerations we know that $\ddot{\tilde{\boldsymbol{q}}}$, $\ddot{\tilde{\boldsymbol{\eta}}}_1, \ddot{\tilde{\boldsymbol{\eta}}}_2$ and therefore $\dot{\boldsymbol{x}}$ are bounded. From (32) it follows that $\|\boldsymbol{f}(t, \boldsymbol{x})\|$ is bounded.

We showed that conditions *(i)-(v)* of Matrosov's Theorem are satisfied. To analyse the region of attraction we can use the upper bound of V from (38). For any starting condition $\boldsymbol{x}_0$ it is possible to find an $\alpha > 0$ such that $V(t, \boldsymbol{x}) \leq a(\alpha)$, meaning that $\boldsymbol{x}_0$ lies within the region of attraction $V_{t,\alpha}^{-1}$. Since we limited Ω to be an arbitrarily large but bounded set we can not reason global stability. However, we showed that the origin $\boldsymbol{x} = \boldsymbol{0}$ is a uniformly asymptotically stable equilibrium point of the closed-loop system (24)-(26).

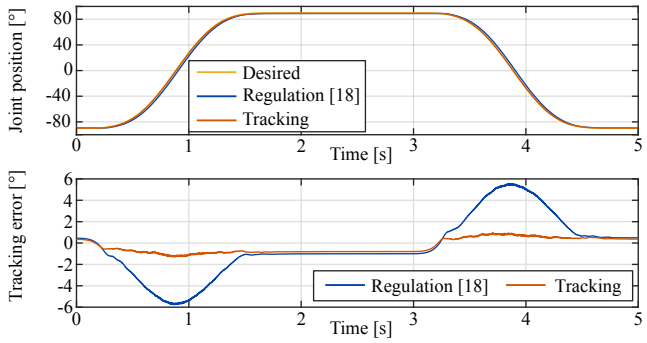

Fig. 3. Desired step-like trajectory and actual joint positions (top). Link-side tracking error (bottom) for the regulation (blue) and tracking (orange) controller.

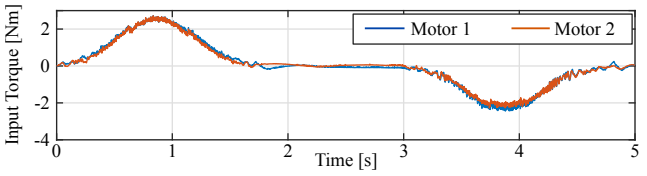

Fig. 4. Input torques of motor 1 and motor 2 for the tracking control and the commanded desired step-like trajectory from Fig. 3.

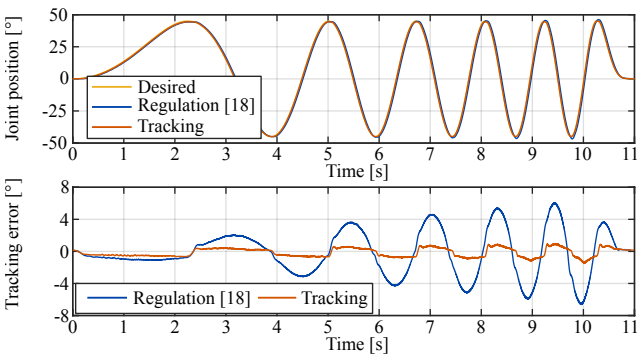

Fig. 5. Desired chirp trajectory and actual joint positions (top). Link-side tracking error (bottom) for the regulation (blue) and tracking (orange) controller.

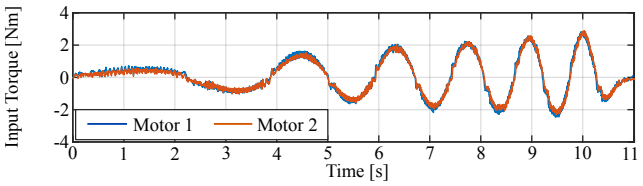

Fig. 6. Input torques of motor 1 and motor 2 for the tracking control and the commanded desired chirp trajectory from Fig. 5.

V. Experimental Validation

To validate the proposed controller, experiments on the forearm-rotation joint of the anthropomorphic robot *David* are conducted, see Fig. 1. Throughout all experiments motor inertia shaping, as presented in [7], has been applied, to reduce the parasitic effect of motor friction. Each entry of the constant motor inertia matrix $\boldsymbol{B}$ is scaled down by a factor of 0.3. Besides that, a motor friction observer was applied to compensate for remaining frictional effects on the motor side. The damping matrices were designed based on modal decomposition as shown in [7]. For the 1-DoF case this means $D_q = 2\xi_q\sqrt{K_q M}$ and $D_{\eta,i} = 2\xi_{\eta,i}\sqrt{K_i B_i}$ for $i = 1, 2$. The modal damping factors were chosen as $\xi_q = 0.2$ and $\xi_{\eta,i} = 0.1$. To demonstrate the benefits of the proposed tracking controller, a comparison with the regulation controller [18] has been performed. For the sake of comparability the parameters K_q, ξ_q, $\xi_{\eta,i}$ and the scaling factor for the motor inertia shaping were always chosen equal for both the regulation and the tracking controller. For the visualization within this chapter all recorded data has been downsampled from 3 kHz to 600 Hz.

A. Link-side tracking behavior

To evaluate the tracking performance a step-like function as desired link-side trajectory has been applied, going from $-90°$ to $+90°$ and back again (Fig. 3). The upper diagram in Fig. 3 shows the desired trajectory together with the actual joint positions achieved with [18] and the proposed controller. For this experiment $K_q = 30\,\mathrm{Nm/rad}$ and $\tau_{0,1} = \tau_{0,2} = 0\,\mathrm{Nm}$ have been chosen. The tracking error $\tilde{q}$ is shown in the bottom diagram of Fig. 3. One can see that the tracking controller is superior in terms of the control performance during the transient. The maximum error is about $1.3°$ (RMSE $0.74°$) for the tracking controller and about $5.8°$ (RMSE $2.75°$) for the regulation controller. The steady-state error in both controllers is comparable with a maximum of about $1°$. A directional dependency of the tracking error can be observed in the transient as well as in the steady state.

The two motors integrated in the considered BAVS joint have a maximum feasible torque of $\pm 4\,\mathrm{Nm}$ each. In the experiments the commanded torque is composed of the computed control action from Section II and the action of the motor friction observer/compensator. The total of both values is visualized in Fig. 4 in case of the tracking controller. One can see that the maximum torque of the motors is not exceeded at any time.

In the second experiment a sine wave from $-45°$ to $+45°$ with variable frequency is commanded as desired link-side trajectory. This trajectory and the actual joint positions are depicted in Fig. 5 (top). In Fig. 5 (bottom) the tracking errors are plotted. As expected, the performance in case of the regulation controller decreases with increasing frequency. This is due to the fact that [18] does not involve any feed-forward terms to compensate for the dynamics necessary to realize the desired link-side trajectory. Interestingly, the maximum tracking errors with the proposed tracking controller are only marginally affected by the increasing frequency in the desired trajectory, confirming the practical applicability also for highly dynamic motions. Fig. 6 demonstrates the corresponding control torques for both motors.

B. Regulation of a desired pretension

In addition to motion tracking, the proposed controller can simultaneously regulate the pretension in the elastic element. This is demonstrated in the following experiment. The preten-

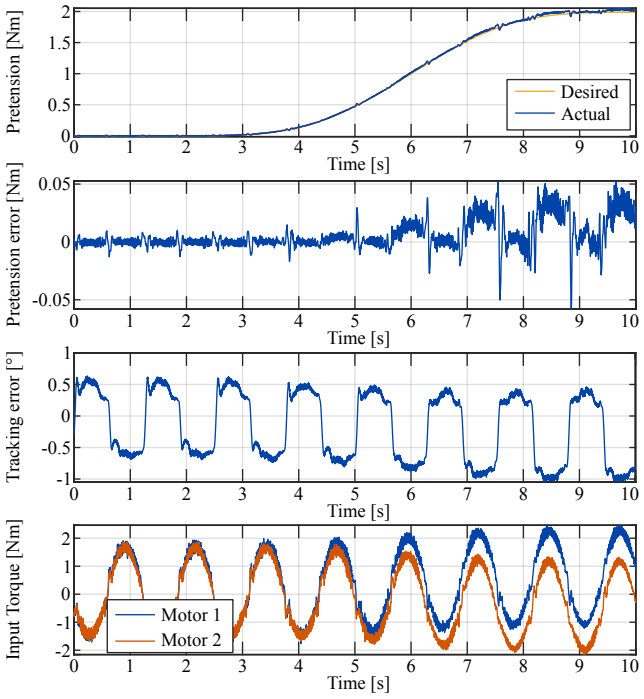

Fig. 7. Desired and actual time-varying pretension profile of the elastic element (top), and the corresponding pretension error as well as the link-side tracking error (middle). Input torques of both motors (bottom).

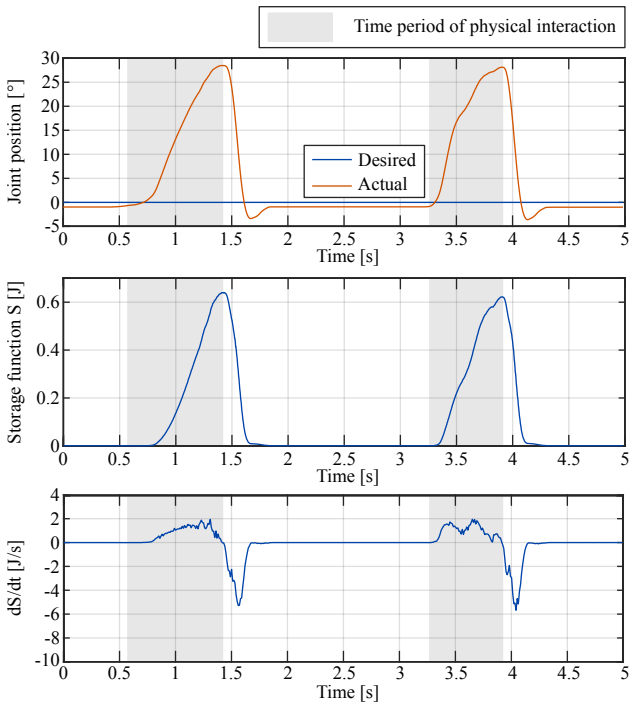

Fig. 8. Desired and actual joint position (top), storage function S (middle) and its time derivative $\dot{S}$ (bottom).

sion was changed from $\tau_{0,1} = 0\,\mathrm{Nm}$ to $\tau_{0,1} = 1\,\mathrm{Nm}$, accordingly $\tau_{0,2}$ from $0\,\mathrm{Nm}$ to $-1\,\mathrm{Nm}$, while the link-side is commanded to track a sine wave with a frequency around $1.3\,\mathrm{Hz}$ from $-30°$ to $+30°$. In this experiment $K_q = 50\,\mathrm{Nm/rad}$ has been selected.

One expects $K_i\varphi_i \to \tau_{0,i}$ for $i = 1, 2$ for $\tilde{q} \to 0$. From (9) it follows that $\tau_1(\varphi_1^\theta) - \tau_2(\varphi_2^\theta) \to \tau_{0,1} - \tau_{0,2}$. According to that, the choice $\tau_{0,\mathrm{d}} = \tau_{0,1} - \tau_{0,2}$ as desired pretension is made and the difference $\tau_1(\varphi_1^\theta) - \tau_2(\varphi_2^\theta)$ represents the actual pretension in the system. Both values are shown in Fig. 7 (top). The difference of both values, referred to as pretension error, is depicted in the second chart in Fig. 7. The experiment shows that it is possible to regulate a given pretension and track a desired link-side trajectory simultaneously. The two bottom diagrams in Fig. 7 illustrate the link-side tracking error and the input torque, respectively. It can be seen that with increasing preload, the tracking behavior deteriorates. One can observe that the directional dependency of the tracking error increases with rising pretension. This effect and the question how it affects the use of the elastic mechanism will be investigated further in future works.

C. Interaction behavior

The last experiment verifies the results of the passivity analysis in Section III. The tracking controller is commanded to keep a constant desired joint position, while the user interacts with the robot, see Fig. 8 (top). The controller gains in the experiments have been chosen as follows: $K_q = 5\,\mathrm{Nm/rad}$, $\xi_q = 0.3$, $\tau_{0,1} = \tau_{0,2} = 0\,\mathrm{Nm}$. The time period of physical interaction is marked in gray. After releasing the link of the robot, the actual joint position returns to the desired one[2]. In the second chart of Fig. 8, the storage function S from Section III is plotted. After the physical interaction, that is, $\tau_{\mathrm{ext}} = 0\,\mathrm{Nm}$, the storage function decreases according to the passivity considerations and the conclusions drawn in Remark 1. For the sake of completeness, the bottom diagram in Fig. 8 shows $\dot{S}$ which stays below zero during free motion.

VI. Conclusion

In this work, we presented a passivity-based controller that achieves simultaneous motion tracking and joint stiffness control for biologically inspired, bidirectional variable-stiffness actuators. In harmony with the ESP design philosophy, we aimed at modifying the intrinsic dynamics to a minimal extent. Passivity and uniform asymptotic stability of the resulting closed-loop dynamics have been formally shown, with the former facilitating robust and compliant interaction with the environment. The proposed controller is evaluated on the forearm BAVS joint of DLR *David*. The experimental results highlight the tracking performance and demonstrate that independent joint stiffness and link position control can be achieved. Finally, passivity of the closed loop is verified in a human-robot interaction experiment.

References

[1] G. A. Pratt and M. M. Williamson, "Series elastic actuators," in *Proceedings 1995 IEEE/RSJ International Conference on Intelligent Robots and Systems. Human Robot Interaction and Cooperative Robots*, vol. 1. IEEE, 1995, pp. 399–406.

[2] apart from the natural steady-state error inherent in all control laws without integral part, which are intended for compliant interaction

[2] S. Wolf *et al.*, "Variable stiffness actuators: Review on design and components," *IEEE/ASME transactions on mechatronics*, vol. 21, no. 5, pp. 2418–2430, 2015.

[3] F. Petit, W. Friedl, H. Höppner, and M. Grebenstein, "Analysis and synthesis of the bidirectional antagonistic variable stiffness mechanism," *IEEE/ASME Transactions on Mechatronics*, vol. 20, no. 2, pp. 684–695, 2014.

[4] B. Vanderborght *et al.*, "Variable impedance actuators: A review," *Robotics and autonomous systems*, vol. 61, no. 12, pp. 1601–1614, 2013.

[5] M. Grebenstein *et al.*, "The dlr hand arm system," in *2011 IEEE International Conference on Robotics and Automation*. IEEE, 2011, pp. 3175–3182.

[6] S. Wolf, O. Eiberger, and G. Hirzinger, "The dlr fsj: Energy based design of a variable stiffness joint," in *2011 IEEE International Conference on Robotics and Automation*. IEEE, 2011, pp. 5082–5089.

[7] M. Keppler, D. Lakatos, C. Ott, and A. Albu-Schäffer, "Elastic structure preserving (esp) control for compliantly actuated robots," *IEEE Transactions on Robotics*, vol. 34, no. 2, pp. 317–335, 2018.

[8] F. Petit, M. Chalon, W. Friedl, M. Grebenstein, A. Albu-Schäffer, and G. Hirzinger, "Bidirectional antagonistic variable stiffness actuation: Analysis, design & implementation," in *2010 IEEE International Conference on Robotics and Automation*. IEEE, 2010, pp. 4189–4196.

[9] M. G. Catalano, G. Grioli, M. Garabini, F. Bonomo, M. Mancini, N. Tsagarakis, and A. Bicchi, "Vsa-cubebot: A modular variable stiffness platform for multiple degrees of freedom robots," in *2011 IEEE international conference on robotics and automation*. IEEE, 2011, pp. 5090–5095.

[10] H. Höppner, W. Wiedmeyer, and P. van der Smagt, "A new biarticular joint mechanism to extend stiffness ranges," in *2014 IEEE International Conference on Robotics and Automation (ICRA)*. IEEE, 2014, pp. 3403–3410.

[11] W. Friedl, H. Höppner, F. Petit, and G. Hirzinger, "Wrist and forearm rotation of the dlr hand arm system: Mechanical design, shape analysis and experimental validation," in *2011 IEEE/RSJ International Conference on Intelligent Robots and Systems*. IEEE, 2011, pp. 1836–1842.

[12] G. Palli, C. Melchiorri, and A. De Luca, "On the feedback linearization of robots with variable joint stiffness," in *2008 IEEE international conference on robotics and automation*. IEEE, 2008, pp. 1753–1759.

[13] A. De Luca, F. Flacco, A. Bicchi, and R. Schiavi, "Nonlinear decoupled motion-stiffness control and collision detection/reaction for the vsa-ii variable stiffness device," in *2009 IEEE/RSJ International Conference on Intelligent Robots and Systems*. IEEE, 2009, pp. 5487–5494.

[14] S. Savin, R. Khusainov, and A. Klimchik, "Control of actuators with linearized variable stiffness," *IFAC-PapersOnLine*, vol. 52, no. 13, pp. 713–718, 2019.

[15] A. De Luca and F. Flacco, "Dynamic gravity cancellation in robots with flexible transmissions," in *49th IEEE Conference on Decision and Control (CDC)*, 2010, pp. 288–295.

[16] J. Guo and G. Tian, "Mechanical design and robust tracking control of a class of antagonistic variable stiffness actuators based on the equivalent nonlinear torsion springs," *Proceedings of the Institution of Mechanical Engineers, Part I: Journal of Systems and Control Engineering*, vol. 232, no. 10, pp. 1337–1355, 2018.

[17] R. Mengacci, M. Keppler, M. Pfanne, A. Bicchi, and C. Ott, "Elastic structure preserving control for compliant robots driven by agonistic-antagonistic actuators (espaa)," *IEEE Robotics and Automation Letters*, vol. 6, no. 2, pp. 879–886, 2021.

[18] X. Meng, M. Keppler, and C. Ott, "Elastic structure preserving impedance control of bidirectional antagonistic variable stiffness actuation," in *European Control Conference 2020, ECC 2021*, 2021, pp. 263–269.

[19] M. Spong, "Modeling and control of elastic joint robots," *Mathematical and Computer Modelling*, vol. 12, no. 7, p. 912, 1989.

[20] F. Ghorbel, B. Srinivasan, and M. W. Spong, "On the uniform boundedness of the inertia matrix of serial robot manipulators," *Journal of Robotic Systems*, vol. 15, no. 1, pp. 17–28, 1998.

[21] R. Murray, Z. Li, S. Sastry, and S. Sastry, *A Mathematical Introduction to Robotic Manipulation*. Taylor & Francis, 1994.

[22] M. Keppler, D. Lakatos, C. Ott, and A. Albu-Schaffer, "Elastic structure preserving impedance (esπ) control for compliantly actuated robots," in *2018 IEEE/RSJ International Conference on Intelligent Robots and Systems (IROS)*. IEEE, 2018, pp. 5861–5868.

[23] V. Matrosov, "On the stability of motion," *Journal of Applied Mathematics and Mechanics*, vol. 26, no. 5, pp. 1337–1353, 1962.

[24] N. Rouche, P. Habets, and M. Laloy, *Stability theory by Liapunov's direct method*. Springer, 1977, vol. 4.

[25] B. Paden and R. Panja, "Globally asymptotically stable pd+ controller for robot manipulators," *International Journal of Control*, vol. 47, no. 6, pp. 1697–1712, 1988.

[26] C. D. Meyer, *Matrix analysis and applied linear algebra*. Siam, 2000, vol. 71.